Infrared Spectroscopic Study of CO Adsorption and Electro-oxidation on Carbon-Supported Pt Nanoparticles: Interparticle versus Intraparticle Heterogeneity

ARTICLE *in* THE JOURNAL OF PHYSICAL CHEMISTRY B · NOVEMBER 2004

Impact Factor: 3.3 · DOI: 10.1021/jp0479163

Infrared Spectroscopic Study of CO Adsorption and Electro-oxidation on Carbon-Supported Pt Nanoparticles: Interparticle versus Intraparticle Heterogeneity

Frédéric Maillard,[†] Elena R. Savinova,*[,†,‡] Pavel A. Simonov,[‡] Vladimir I. Zaikovskii,[‡] and Ulrich Stimming[†]

Technische Universität München, Department of Physics E19, James-Franck-Str. 1, D-85748 Garching, Germany, and Boreskov Institute of Catalysis, Pr. Akademika Lavrentieva 5, 630090 Novosibirsk, Russian Federation

Received: May 15, 2004; In Final Form: August 26, 2004

In this paper, we use Fourier transform infrared (FTIR) spectroscopy and stripping voltammetry at saturation and submonolayer CO coverages to shed light on the influence of size on the CO adsorption and electro-oxidation on Pt nanoparticles. Pt nanoparticles supported on low surface area ($\sim$1 m^2 g^{-1}) carbon (Sibunit) are used throughout the study. The vibrational spectra of adsorbed CO are dominated by interparticle heterogeneity (contribution of particles of different size in the range from 0.5 to 5 nm) rather than intraparticle heterogeneity (contribution of different adsorption sites). CO stripping voltammetry exhibits two peaks separated by approximately 0.25 V (at 0.02 V s^{-1}), which are attributed to the CO oxidation from "large" ($\sim$3.6 nm) and "small" ($\sim$1.7 nm) Pt nanoparticles. Using stepwise oxidation, we were able to separate the contributions of "large" and "small" nanoparticles and obtain their infrared and voltammetric "fingerprints". Considerable differences are observed between "large" and "small" nanoparticles in terms of (i) the vibrational frequencies of adsorbed CO molecules (ii) their vibrational coupling, and (iii) CO oxidation overpotential.

1. Introduction

Investigation of particle size effects attracts an increasing attention of the surface science and electrochemical communities (see, e.g., review articles in *Catalysis & Electrocatalysis at Nanoparticle Surfaces*[1]). CO monolayer oxidation is one of the most widely explored surface reactions at both the solid/gas and the electrified solid/liquid interfaces. Considerable differences have recently been observed between CO oxidation at metal nanoparticles and at extended surfaces, both at the solid/gas[2−6] as well as the solid/liquid interfaces.[7−10] In the case of electrochemical CO oxidation, the overpotential increases considerably as compared to extended surfaces, and the reaction kinetics changes with a decrease in the particle size below approximately 3 nm. The reason for the reduced catalytic activity of metal nanoparticles versus extended surfaces is not clear yet. The most extensively discussed hypothesis ascribes slower CO oxidation on nanoparticles to the high ratio of low coordinated sites (edges and corners), which adsorb both CO and the second reaction partner, oxygen containing species, stronger.[2−6,11]

Recently, Guerin et al.[12] observed two voltammetric peaks upon CO oxidative stripping from commercial Pt/Vulcan catalysts and ascribed the peak at more negative potentials to the CO oxidation on terraces while attributing the more positive one to the CO oxidation on particle edges. Zdhanov and Kasemo[13] simulated a CO stripping voltammogram from a nanometer-sized supported Pt crystallite exhibiting (111) and (100) facets and showed that the voltammetric peak will indeed split into two if CO diffusion between the facets is hindered. On the other hand, Friedrich et al.[7] attributed multiple peaks in CO stripping voltammograms from Pt colloidal particles immobilized on a Au substrate to CO oxidation on nanoparticles of different size. It is therefore important to clarify whether the (i) intraparticle or (ii) interparticle heterogeneity is dominating the behavior of nanosized metal particles. The first hypothesis considers a nanoparticle as a sum of the adsorption sites (high coordinated terrace and low coordinated edge) it comprises. If this is true, the behavior of nanoparticles is likely to be similar to that of high index single crystals with high step density. The second hypothesis is based on the assumption that a decrease of particle size does not only influence the contribution of different facets and increase the ratio between high and low coordination sites on its surface, but due to electronic effects also changes the properties of a particle as a whole. This means that a Pt atom with the coordination number 9, belonging to a (111) facet of a 1 nm particle, will have properties different from a Pt atom with the same coordination number but belonging to a (111) facet of, say, a 5 nm particle. At present, the first hypothesis dominates in the surface science and catalysis,[2−6] as well as in the electrochemical,[11,12] communities. It appears surprising that very few studies take into account the particle size distribution when analyzing the behavior of supported metal electrocatalysts. Meanwhile, size distribution is an immanent property of a statistical ensemble of nanometer-size metal particles, and it must be taken into consideration.

IR spectroscopy has proven to be useful in shedding light on the mechanism of CO oxidation on Pt single crystalline surfaces both at solid/gas[14,15] and at electrified solid/liquid interfaces.[16−18] IR spectra of CO adsorbed on metal surfaces at saturation coverage are dominated by dipole−dipole coupling of the adsorbed molecules, resulting in blue shifts of the absorption bands and intensity borrowing from low frequency to high frequency vibrations. Decreasing the density of dipoles (i.e., decreasing the adsorbate coverage) lifts vibrational coupling and

* Corresponding author. Tel: +7 3832 34 25 63. Fax: +7 3832 34 30 56. E-mail: elensav@catalysis.ru.
[†] Technische Universität München.
[‡] Boreskov Institute of Catalysis.

10.1021/jp0479163 CCC: $27.50
Published on Web 10/26/2004

delivers a wealth of information concerning the adlayer structure, the adsorbate island formation, and the contribution of step and terrace sites to CO bonding.[16,18−21]

Recently, investigation of the CO adsorption on metal nanoparticles using vibrational spectroscopies became a rapidly emerging field. Friedrich et al. pioneered application of FTIR spectroscopy to first probe colloidal Pt particles immobilized on gold,[7] and then carbon-supported Pt particles adhesively attached to a gold electrode.[22] The latter approach was then adopted by Park and co-workers.[23−25] Considerable shifts of the CO stretching frequency with the decrease of the particle size were observed in these experiments. These were interpreted in terms of an increased electron back-donation from metal d-orbitals into CO $2\pi^*$ orbitals for smaller particles.[26] For particles above 4 nm in size, the CO stretching frequency approached the value characteristic of CO adsorbed on Pt(111) single crystals.[23]

In this paper, we make use of vibrational spectroscopy and stripping voltammetry to investigate absorption and electrochemical oxidation of CO on carbon-supported Pt nanoparticles. We use Pt nanoparticles prepared through a chemical route and supported on a low surface area ($\sim$1 m^2 g^{-1}) Sibunit carbon. To avoid "anomalous" optical effects described, for example, by Park et al.,[24] and Pecharromán et al.,[27,28] a thin film of the catalyst is adhesively attached to the highly reflective gold substrate using a procedure similar to that described by Friedrich et al.[22] and Park et al.[24] and employed as an electrode. We explore CO adlayers at saturation and at submonolayer coverages obtained by dosing as well as by CO stepwise oxidation. The experimental results for Pt nanoparticles are compared with literature data for extended surfaces and analyzed in terms of interparticle as well as intraparticle heterogeneity. We show that neglecting particle size distribution may result in misinterpretation of the IR spectra of CO chemisorbed on supported nanoparticles.

2. Experimental Section

Nanoparticle Preparation and Characterization. Pt nanoparticles were supported on Sibunit, a carbon with a specific surface area of $\sim$1 m^2g^{-1}. Carbons of the Sibunit family are prepared through pyrolysis of natural gases on carbon black surfaces followed by an activation to achieve desired values of the surface area and pore volume.[29] Pyrolysis leads to formation of dense graphitelike deposits, and in the course of the activation procedure the carbon black component is removed first. Hence, the pore size distribution in the final Sibunit sample roughly reproduces the particle size distribution in the carbon black precursor. Thus, varying the type of the gas source, the template (carbon black), and the manner and duration of the activation, enables production of meso- or macroporous carbon materials with surface areas from 1 to 50 (nonactivated) to 50−500 m^2 g^{-1} (activated) and pore volume up to 1 cm^3 g^{-1}. The advantage of carbons of the Sibunit family is their purity, high electrical conductivity, and the uniform morphology of primary carbon globules (contrary to carbon blacks, in particular Vulcan[30]).

Pt supported on Sibunit (Pt/Sibunit) was prepared via the polyhydroxocomplex route using an approach similar to that described by Simonov et al.[31] for preparation of carbon-supported palladium catalysts. Carbon powder and K_2PtCl_4 solution were mixed and agitated for 20 min at room temperature. After heating the slurry to 80 °C, Na_2CO_3 solution was added to it (end point pH 6) to precipitate platinum hydroxide species. The catalyst precursors were aged for 1 h, then the slurry was allowed to cool. Subsequent filtering, washing with Milli-Q water, drying at 110 °C, and reducing with H_2 at 300 °C (1 h) gave rise to the final 5 wt. % Pt/Sibunit catalyst.

The catalyst was examined with high resolution transmission electron microscopy (HRTEM) using a JEOL-2010 instrument. To determine the surface average particle size $\overline{d_S}$, approximately 800 particles were counted and the following formula was applied:

$$\overline{d_S} = \sum_i N_i d_i^3 / \sum_i N_i d_i^2$$

with N_i as the number of particles with a diameter d_i.

Electrode Preparation. Polycrystalline Au disks (Mateck) were polished to a mirror finish and flame annealed before each experiment. Working electrodes were prepared by depositing a desired amount of Pt/Sibunit suspended in water on a gold disk and drying in air using a procedure similar to that described by Friedrich et al.[22] and Park et al.[24] An excess of the catalyst, weakly attached to the gold substrate, was removed by rinsing the electrode under a strong Milli-Q water flow. The resulting films were mechanically stable and showed reproducible cyclic voltammograms (CVs) and IR spectra. Care has been taken to obtain thin and "homogeneous" catalyst films on the Au substrate and thus minimize "anomalous" optical effects, resulting in negatively pointing CO absorption bands. The latter are due to the complex refractive behavior of metal particles deposited on poorly reflecting substrates (e.g., carbon) and depend on the light incidence angle, polarization, and the fill factor of metal particles, that is, the volume fraction of the thin layer occupied by metal particles. These issues have been discussed in detail by Pecharromán et al.[27,28]

After each experiment, Pt/Sibunit was removed from the gold substrate by wiping the surface under a water flow. To ensure that no Pt catalyst remained on the gold surface from the previous experiment, the CV of the Au electrode was recorded before each new deposition.

Electrochemical Measurements. Solutions were prepared from Milli-Q water (18 MΩ·cm), $HClO_4$ (Suprapur, Merck), and H_2SO_4 (Suprapur, Merck). Electrochemical measurements were carried out in a three-electrode cell at room temperature in an Ar atmosphere. The cell was cleaned before every experiment by soaking it overnight in a H_2SO_4/H_2O_2 mixture. The counter electrode was a Pt foil and the reference electrode was a reversible hydrogen electrode (RHE) connected to the cell via a Luggin capillary. Potential values below are given on the RHE scale. Prior to the measurements, the working electrode potential was cycled between 0.03 and 1.23 V at a 0.1 V s^{-1} scan rate to clean the Pt surface and obtain stable cyclic voltammograms. CO adsorption was performed at 0.1 V. To achieve saturation coverage, CO was bubbled through the electrolyte for 1 min, and then the electrolyte was purged with Ar for 1 h to ensure that no dissolved CO remained in the bulk of the electrolyte (15 cm^3 volume). This let sufficient time for the adlayer to equilibrate. These conditions have proven to result in saturation CO coverage and highly reproducible stripping voltammograms. Submonolayer CO coverages were achieved by adsorption from diluted CO solutions (obtained by adding specified amounts of CO-saturated electrolyte into the electrochemical cell) for 5 min at 0.1 V and purging with Ar for 1 h to remove dissolved CO and allow the CO adlayer to equilibrate.

The Pt surface area was determined by hydrogen UPD (assuming 210 μC cm^{-2}) and CO stripping voltammetry (assuming 420 μC cm^{-2}). These procedures showed good agreement (within ±10%), evidencing 1:1 stoichiometry of

H/CO adsorption. Current densities are referred to a cm^2 of Pt. The fractional adsorbate coverage X_{CO} was determined relative to the amount of CO attained under saturation conditions ($X_{CO} = 1$).

Infrared Spectroscopy. FTIR measurements were performed under external reflection conditions in a thin layer configuration using a Bio Rad FTS 6000 spectrometer with a self-designed cell attachment and *p*-polarized light. The spectroscopic cell was made from Duran glass with a CaF_2 prism beveled at 60° and attached to the bottom of the cell. The detector was liquid-N_2-cooled MCT. To obtain a single-beam spectrum, 800 interferograms acquired at a spectral resolution of 4 cm^{-1} were coadded and then Fourier transformed. All spectra were collected at 0.1 V to avoid the effect of the electrode potential on the CO stretching frequency (Stark effect) and facilitate interpretation of an albeit complex IR spectra. Special experiments were carried out, which proved that neither readsorption of CO from solution nor reduction of CO_2 trapped in the thin layer occurred during the spectra acquisition at 0.1 V. The IR absorption spectra were calculated as changes in the reflectivity (R_i) using the formula

$$\frac{\Delta R}{R} \times 100\% = \frac{R_i - R_{ref}}{R_{ref}} \times 100$$

R_{ref} corresponds to a reference single-beam spectrum, which was collected at the end of each experiment by stepping the potential to +1.2 V for 60 s, and thus oxidizing all adsorbed CO molecules, and then stepping back to 0.1 V.

Special experiments were performed, which confirmed an absence of CO adsorption on the gold substrate under the experimental conditions employed. This is in accordance with previous publications, which prove that CO adsorption on Au requires higher CO concentrations and longer adsorption times.[7,32]

For dosing experiments, X_{CO} was calculated using stripping voltammetry by integrating the CO oxidation peak and relating the charge obtained to the charge attained under saturation conditions. For CO adlayers prepared by oxidative stripping, X_{CO} was estimated from the integrated intensity of the absorption band of a-top CO. Although this procedure must be used with caution due to the influence of dipole−dipole coupling on the IR intensity, it has proven to provide a satisfactory in situ estimate of the CO coverage.[19] Unfortunately, calculating CO fractional coverage from the absorbance of CO_2 at 2345 cm^{-1} was not always possible, since CO_2 formed via CO oxidation was slowly escaping from the thin layer during long IR experiments.

3. Results and Data Analyses

3.1. TEM Characterization. TEM images of the catalyst under different magnifications are represented in Figure 1. The particle size distribution is shown in Figure 2a. The surface average particle size $\overline{d_S}$ equals 3.4 nm with a relative standard deviation of 44%. The latter is typical for supported metal nanoparticles, which usually demonstrate marked distributions. Indeed, the relative standard deviations calculated from the particle size distributions reported by Maillard et al.[33] for E-TEK catalysts were equal to 28, 51, 37, and 36% for Pt/Vulcan (XC72−Cabot) containing 10, 20, 30, and 40% Pt, respectively. It is remarkable that the particle size distribution shown in Figure 2a is bimodal and exhibits two maxima at d ∼ 1.7 nm and d ∼ 3.6 nm crystallite size. Although the number of "small" (∼1.7 nm) particles amounts to approximately 52% of the total number

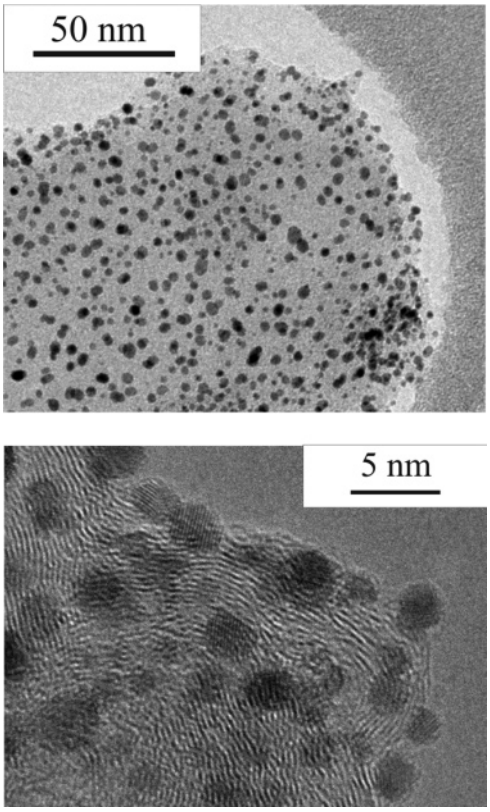

Figure 1. TEM (top) and HRTEM (bottom) images of 5% Pt/Sibunit.

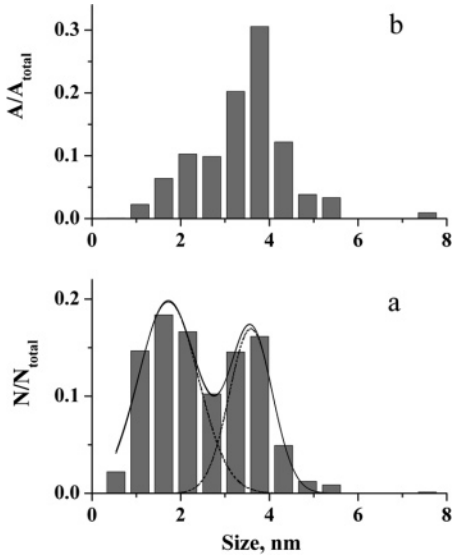

Figure 2. (a) Particle size and (b) area distributions for 5% Pt/Sibunit reconstructed from TEM images.

of particles, their contribution to the overall Pt surface area amounts to only approximately 19%. The surface distribution is represented in Figure 2b. In the following sections we will show that the bimodal size distribution makes the catalyst particularly suited for probing the influence of interparticle heterogeneity.

The high resolution TEM image of Pt/Sibunit is shown in Figure 1 (bottom). The metal lattice can be clearly discerned for particles above ∼2 nm, evidencing, in agreement with previous publications,[34,35] that Pt nanoparticles are faceted single crystals. The microdiffraction data confirms the fcc structure of metal particles. However, for particles of $d \leq 1$ nm it was not possible to visualize the crystalline lattice, which may be due to a distortion of their crystalline lattice.

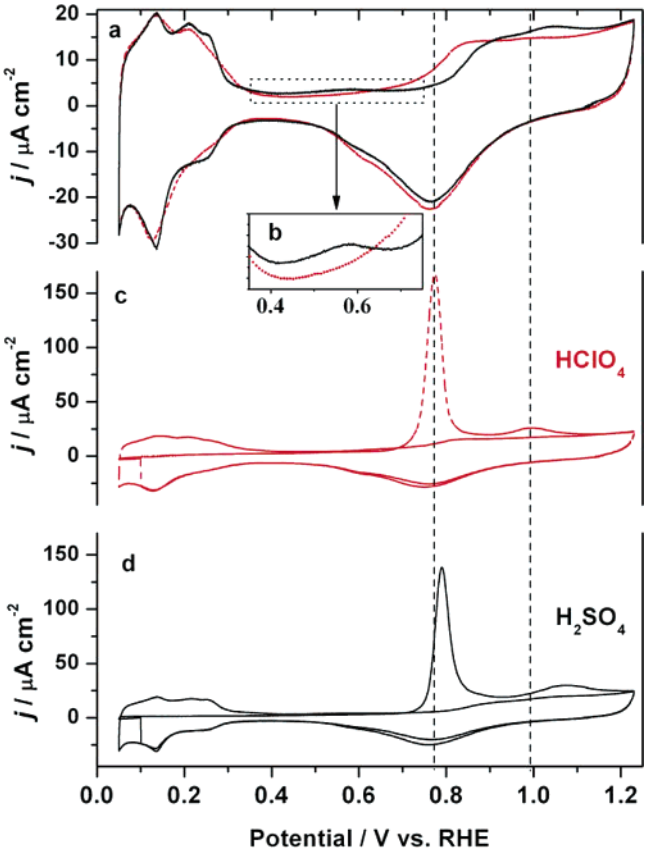

Figure 3. (a) CVs and (c), (d) CO stripping voltammograms in 0.1 M H_2SO_4 (solid line, black) and 0.1 M $HClO_4$ (dashed line, red) at the sweep rate of 0.02 V s^{-1}. (b) Zoom of the potential region corresponding to (bi)sulfate adsorption. CO adsorption potential 0.1 V vs RHE, T = 298 K.

3.2. CO Stripping Voltammetry. *3.2.1. Oxidation of CO at Saturation Coverage*. Most of the measurements in this work were performed in $HClO_4$ to avoid the influence of specific anion adsorption. However, some experiments were made in H_2SO_4, in order, first, to compare our data to the literature (since H_2SO_4 is often used as a supporting electrolyte) and, second, to find out whether (bi)sulfate adsorption has an influence on the vibrational spectra of CO adsorbed on Pt nanoparticles and its oxidation overpotential.

We first analyze CVs in CO-free solutions represented in Figures 3a and 3b. A wide peak is clearly discernible in the inset (Figure 3b) between ~0.4 and 0.7 V in the CV in H_2SO_4, and is absent in $HClO_4$, which allows attributing it to specific adsorption of (bi)sulfate on Pt nanoparticles. The position of the peak on the potential scale is similar to that reported for Pt(111) (see e.g. refs 36, 37 and references therein). However, the current spike featured by Pt(111) and, according to Funtikov et al.,[38] corresponding to an order/disorder phase transition and formation of the $(\sqrt{3} \times \sqrt{7})R30°$ adlayer structure, is absent in the CV of the Pt/Sibunit catalyst. The latter is consistent with the small size of facets on the surface of 3.6 and 1.7 nm nanoparticles. Indeed, the phase transition requires long-range order and, hence, has not been detected for stepped Pt[n(111) × (110)] or Pt[n(111) × (100)] single crystals even with n = 10.[39,40] On Pt(100) and Pt(110), due to a lower potential of zero charge, the (bi)sulfate adsorption is shifted negative on the potential scale. To our knowledge, this paper provides the first observation of (bi)sulfate adsorption on carbon-supported Pt nanoparticles. The fact that it has not been reported earlier may be attributed to the high specific surface area and concomitant large double layer capacitance of commercial carbon blacks used as supports for fuel cell catalysts. As indicated earlier, the specific surface area of the Sibunit support used in this work amounts to only ~1 m^2 g^{-1}. The oxygen adsorption in H_2SO_4 is shifted approximately 60 mV positive versus that in $HClO_4$, which is apparently due to (bi)sulfate adsorption. Changes are observed also in the hydrogen UPD region, the adsorption/desorption peaks at ~0.25 V being suppressed in the presence of (bi)sulfate.

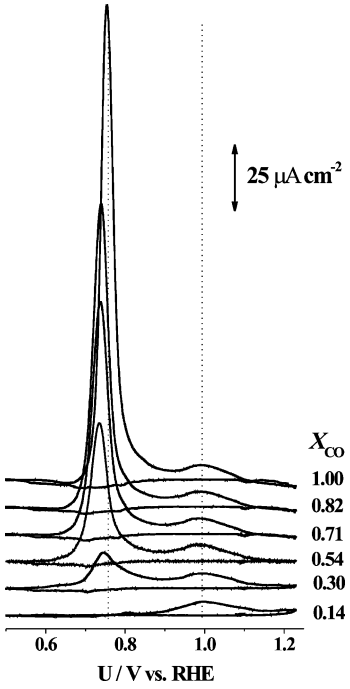

Figure 4. Background corrected CO stripping voltammograms in 0.1 M $HClO_4$. The CO fractional coverage X_{CO} is indicated next to the curves and was established by stepping to 0.7 V RHE for various times. Sweep rate 0.02 V s^{-1}, CO adsorption potential 0.1 V vs RHE, T = 298 K.

The CO stripping voltammogram for Pt/Sibunit in $HClO_4$ represented in Figure 3c shows two oxidation peaks. The low potential peak (LPP) is observed at an electrode potential characteristic of CO stripping from bulk polycrystalline Pt, while the high potential peak (HPP) is located approximately 0.25 V more positive. In the presence of sulfate (Figure 3d) the LPP shifts positive by 20 mV, while the HPP shifts positive by approximately 80 mV (cf. 60 mV shift of oxygen adsorption). Two separate CO stripping peaks in remarkably different potential intervals are indicative of two different CO populations on the investigated catalysts. Let us name the population oxidized under the LPP CO(1) and the one oxidized under the HPP CO(2). Their origin will be further analyzed in the discussion section in terms of the interparticle and intraparticle heterogeneity.

3.2.2. CO Adlayers Prepared by Stepwise Oxidation. The following experimental protocol was employed to generate fractional CO coverages. Saturation CO coverage was obtained at 0.1 V, then part of CO monolayer was oxidized via stepping to a constant potential of 0.7 V for different time periods (from 5 to 300 s), and then CO remaining on the surface was oxidized in a potential sweep. Background-corrected stripping voltammograms for different CO fractional coverages obtained using the above procedure are shown in Figure 4. The LPP gradually shifts negative, as the CO coverage is decreased down to X_{CO} = 0.71, while the HPP stays unchanged. The magnitude of the shift of the LPP component is rather small and amounts to 15

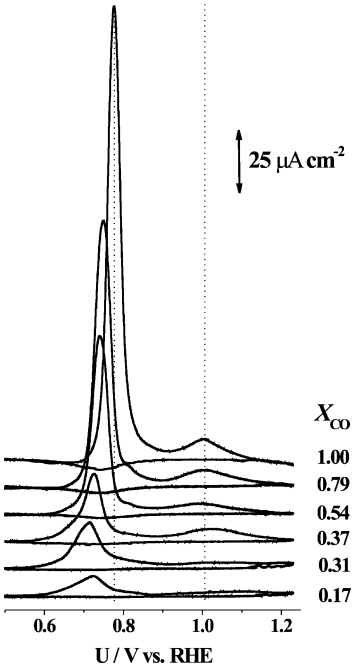

Figure 5. Background corrected CO stripping voltammograms in 0.1 M $HClO_4$. The CO fractional coverage X_{CO} was established by CO dosing from diluted solutions (see Experimental Section for details) and is indicated next to the curves. Sweep rate 0.02 V s^{-1}, CO adsorption potential 0.1 V vs RHE, $T = 298$ K.

mV at $X_{CO} = 0.71$. As the coverage is further decreased, no more negative shift is observed, and the LPP is shifted slightly positive. The charge under the LPP decreases, as more and more CO is removed from the surface in the preceding potential step, while the charge under the HPP stays unchanged. Ultimately, after stepping to 0.7 V for 300 s (X_{CO} is decreased down to 0.14), the LPP disappears and only HPP is observed in the stripping voltammogram. This strongly suggests that HPP and LPP correspond to independent CO populations and there is no "communication" between them.

3.2.3. CO Adlayers Prepared by Dosing. Stripping voltammograms for submonolayer CO coverages obtained by solution dosing are shown in Figure 5. Similar to the behavior observed upon stepwise oxidation, the LPP gradually shifts negative as X_{CO} decreases, although the magnitude of the shift is somewhat higher. Hence, the LPP shifts from 0.77 V at $X_{CO} = 1.0$ to approximately 0.72 V at $X_{CO} = 0.17$. The onset of CO oxidation (which we define as a potential at which current attains 10% of the maximum peak current) also decreases by approximately 100 mV. The position of the HPP does not depend on the coverage in the interval from 1.0 to 0.17. At fractional coverages below 0.17, the amount of charge under the HPP is small and it is not possible to determine the exact peak position. The fact that the LPP shifts for CO fractional coverages obtained by dosing are larger than for those prepared by oxidative stripping is in line with the data reported for Pt single crystal surfaces.[16,41] This was attributed to the smaller size of CO islands under CO dosing conditions. However, the amplitudes of the peak shifts observed upon the decrease of CO coverage for extended surfaces[16,41,42] are much higher than those found here for nanoparticles, both under dosing as well as under oxidative stripping conditions. The most remarkable changes have been observed for Pt(111) and consisted of splitting the single CO stripping peak into three peaks and shifting the onset of CO oxidation negative by more than 0.2 V upon the decrease of CO coverage. Changes produced by decreasing X_{CO} for stepped

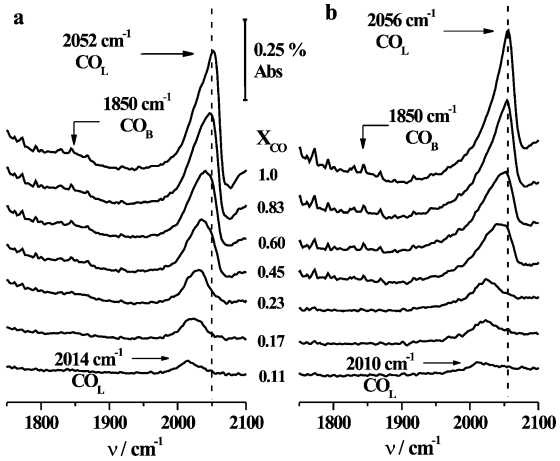

Figure 6. FTIR spectra collected at 0.1 V vs RHE for different CO fractional coverages X_{CO} (as indicated in the graph) in 0.1 M $HClO_4$ (a) and in 0.1 M H_2SO_4 (b). The fractional coverages were established by stepwise oxidation of the CO monolayer (see text for details). The reference spectrum was collected at 0.1 V vs RHE after oxidizing CO at 1.2 V vs RHE for 60 s. CO adsorption potential 0.1 V vs RHE, $T = 298$ K.

Pt[n(111) × (111)] crystals were much smaller.[42] The latter observation has been rationalized in terms of the absence of a competition between CO and OH due to their tentative adsorption at different surface sites.

It should be stressed that in contrast to the behavior observed upon stepwise oxidation, the intensities of both (LPP and HPP) stripping peaks increase simultaneously as more and more CO is dosed to the surface. This means that upon dosing both types of adsorption sites are filled in parallel rather that in sequence.

3.3. FTIR Spectroscopy. *3.3.1. CO Adlayers Prepared by Oxidative Stripping.* FTIR spectra collected in $HClO_4$ and in H_2SO_4 electrolytes are shown in Figure 6. Let us first concentrate on the CO vibrational spectrum at saturation coverage acquired in $HClO_4$ at 0.1 V. The spectrum is dominated by the band corresponding to the a-top CO_{ads} at $\nu_{CO_L} = 2054$ cm^{-1}. This wavenumber is in agreement with the value of 2050 cm^{-1} reported by Friedrich et al.[22] for 10% Vulcan-supported Pt E-TEK catalyst at 0.08 V versus RHE and 2059 cm^{-1} reported by Park et al.[23] for Vulcan (XC72−Cabot) supported 3.5 nm Pt nanoparticles (from E-TEK) at 0.0 V versus Ag/AgCl. High intensity of the a-top peak is usually ascribed to dipole−dipole coupling between adsorbed CO molecules. The bandwidth is rather high and equals approximately 42 cm^{-1}, which is in agreement with the previous observations for supported Pt nanoparticles.[22,23] The considerably larger bandwidth observed for metal nanoparticles compared to single crystal surfaces is usually ascribed to particle heterogeneity. Along with a-top CO, a broad band is observed at $\nu_{CO_B} \approx 1850$ cm^{-1}, which is ascribed to the bridge-bonded CO. Small downward peaks at the high energy side of ν_{CO_L} noticeable in Figure 6a (spectra at high CO coverages) and some of the figures further in the text indicate some interference of the "abnormal" optical effects mentioned above. However, these were kept to a minimum and hence did not influence the data analyses.

Stepwise CO oxidation was achieved by first stepping to 0.7 V for different time intervals until the coverage attained 0.17. Further exposure of the electrode to 0.7 V had no effect on the CO coverage, signaling that the CO(1) population corresponding to the LPP of the CV was fully removed from the particle surface (in agreement with the voltammetry data given in Section 3.2.2). Then, the electrode potential was stepped to 0.95 V to oxidize the CO(2) population corresponding to the HPP

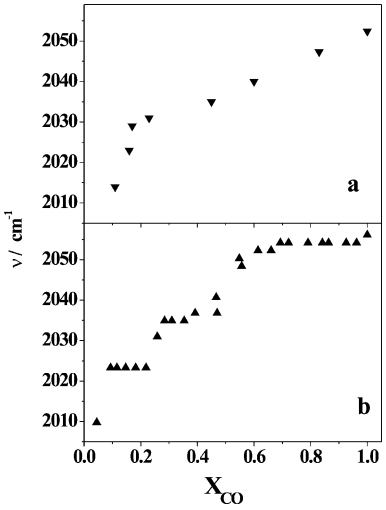

Figure 7. Plot of a-top CO wavenumbers as a function of CO fractional coverage acquired by stepwise oxidation of the CO monolayer. The spectra were collected at 0.1 V vs RHE in 0.1 M $HClO_4$ (a) and in 0.1 M H_2SO_4 (b).

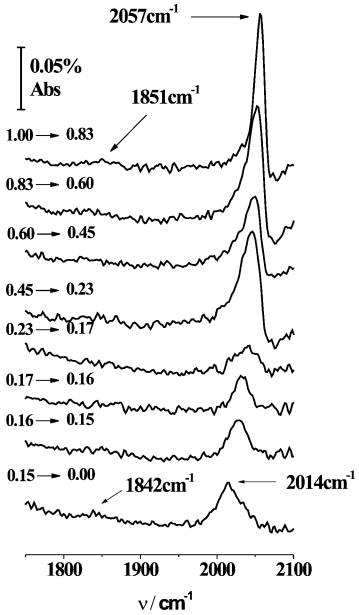

Figure 8. Difference spectra obtained under stepwise oxidation conditions from a saturated CO monolayer by ratioing the single-beam IR spectrum acquired after the *n*-potential step to the single-beam IR spectrum acquired after the $n+1$ step. Variation of the fractional coverage X_{CO} was achieved by first stepping at 0.7 V vs RHE for 20 s (X_{CO}: 1.00 → 0.83), 20 s (X_{CO}: 0.83 → 0.60), 20 s (X_{CO}: 0.60 → 0.45), 60 s (X_{CO}: 0.45 → 0.23), 180 s (X_{CO}: 0.23 → 0.17), and then at 0.95 V vs RHE for 10 s (X_{CO}: 0.17 → 0.16), 20 s (X_{CO}: 0.16 → 0.15), and finally at 1.2 V vs RHE for 60 s (X_{CO}: 0.15 → 0.00). The spectra were collected at 0.1 V vs RHE in 0.1 M $HClO_4$; CO adsorption potential 0.1 V vs RHE; $T = 298$ K.

and to further decrease the coverage. The results for $HClO_4$ are represented in Figure 6a and show that stepwise CO oxidation leads to (i) a decrease in the intensities of the absorption bands of a-top and bridge-bonded CO, (ii) a change in the shape of the former and (iii) its concomitant red shift from 2054 to 2014 cm^{-1}. The spectra in H_2SO_4 are similar, although the band of the bridge-bonded CO appears less pronounced.

Although dipole−dipole coupling between a-top and multifold CO precludes estimation of their relative populations from the intensities of the IR bands,[43] simultaneous decrease of the IR intensities at 2054 and at 1850 cm^{-1} strongly suggests that both a-top and bridge-bonded CO are removed from the surface of Pt nanoparticles simultaneously upon stepwise oxidation. This speaks against the hypothesis proposed by Cairns et al.,[44] who, based on ^{13}C NMR results, concluded that bridge-bonded CO was formed on the surface of carbon-supported Pt nanoparticles as a consequence of partial oxidation of linearly bonded CO. These authors proposed that formation of bridge-bonded CO facilitates oxidation of a-top CO and is thus responsible (at least partly) for the negative shift in the CO stripping onset potential upon stepwise CO monolayer oxidation. Our results do not support this explanation.

The evolution of the wavenumber of a-top CO upon its oxidation in both electrolytes is plotted in Figure 7. One may see that the ν_{CO_L} versus X_{CO} plot in $HClO_4$ can be represented by two linear sections of considerably different slopes, the first ranging from $X_{CO} = 1.0$ to 0.17 and the second from $X_{CO} =$ 0.17 to 0. Obviously, the low frequency band, which features a higher ν_{CO_L} versus X_{CO} slope, corresponds to the CO(2) population oxidized at high overpotentials. In sulfuric acid there is little ν_{CO_L} change from $X_{CO} = 1.0$ to 0.6, while at low X_{CO} the plots in two electrolytes are similar.

Of interest in this paper is also the understanding of the CO oxidation kinetics on nanoparticles. This information is difficult to obtain from the spectra represented in Figure 6, since they reflect which population of CO is remaining on the Pt surface after the potential step, but not which type of CO is oxidized during the step. To obtain the information on the latter we calculate the "difference" absorption spectra by ratioing the single-beam spectrum acquired after the *n*-potential step to the single-beam spectrum acquired after the $n + 1$ step. Note, that although this experimental tactic may seem similar to the one exploited in PDIR (potential difference infrared spectroscopy), their inherent difference comes from the fact that in our case all the spectra are collected at the same electrode potential (0.1 V). This allows avoiding the influence of the vibrational Stark effect and results in unipolar absorption spectra represented in Figure 8 (Small downward peak at high frequency is due to the "abnormal" optical effects mentioned above). Let us follow the changes in the difference spectra upon stepwise CO oxidation. The first spectrum corresponds to the coverage decrease from 1.0 to 0.83 ML and features a very narrow CO_L band at a rather high wavenumber $\nu_{CO_L} = 2057$ cm^{-1}. Carbon monoxide oxidized in the following steps is characterized by a decreased wavenumber and increased width, which are plotted in Figure 9, parts a and b, versus the CO fractional coverage. After the CO(1) population is oxidized, and the electrode potential is stepped to 0.95 V in order to oxidize the CO(2) population, as described above, the peak width of the difference spectrum drops abruptly (Figure 9b). The following stepwise oxidation of CO-(2) is characterized by broadening the CO_L band in the difference spectrum and its red shift (similar to the behavior exhibited by CO(1) population).

3.3.2. CO Adlayers Prepared by Dosing. The evolution of CO spectra obtained upon CO dosing is represented in Figure 10a. The decrease of the coverage results in splitting the absorption band of a-top CO into two components. At low coverage ($X_{CO} \leq 0.17$), the high frequency band disappears, while the low frequency band remains. From the first glance, this spectral behavior resembles very much that observed for stepped single crystal surfaces as a result of lifting dipole−dipole coupling between CO adsorbed on terrace and step sites.[17] It is thus tempting to conclude that it is intraparticle heterogeneity that is dominating the spectra in Figure 10a. The following discussion will, however, bring us to the conclusion that this interpretation is not correct.

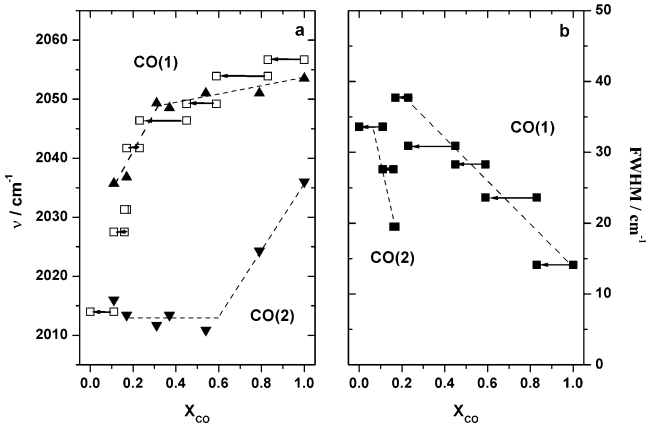

Figure 9. (a) Plots of a-top CO wavenumbers as a function of CO fractional coverages X_{CO}. Filled symbols correspond to the contributions of CO(1) (up triangles) and CO(2) populations (down triangles) under CO dosing conditions; open symbols, to the difference spectra of Figure 8. The arrows indicate the coverage variations during the oxidation steps. (b) Variation of the full width at half-maximum (fwhm) in the difference spectra of Figure 8. FTIR spectra were acquired at 0.1 V vs RHE in 0.1 M $HClO_4$, CO adsorption potential 0.1 V vs RHE, T = 298 K. The lines are guides for the eye.

Since oxidation of the two CO populations occurs at grossly different potential intervals, it is possible to isolate them and obtain their IR fingerprints. The following experimental protocol has been employed. Different CO fractional coverages were achieved on Pt nanoparticles by dosing (see the Experimental Section), and then a single-beam IR spectrum was collected (Spectrum 1). CO(1) was then oxidized by stepping to 0.7 V for 300 s. As stated above, this was sufficient for complete oxidation of the CO(1) population. Longer stepping to 0.7 V produced no changes either in the IR spectrum or in the following stripping CV. After that, the potential was stepped back to 0.1 V and the single-beam IR spectrum was collected (Spectrum 2). Then, the remaining CO(2) population was oxidized in a potential step to 1.2 V for 60 s, and a reference single-beam spectrum was acquired after stepping back to 0.1 V (Spectrum 3). To obtain the fingerprint of CO(1), Spectrum 1 was ratioed to Spectrum 2, while for the fingerprint of CO(2) Spectrum 2 was ratioed to Spectrum 3. The result is shown in Figure 10, parts b and c, and evidences considerably different spectral characteristics and coverage dependences for the CO(1) and CO(2) populations. The influence of the coverage on the CO vibrational frequencies of two CO populations is represented in Figure 9a (filled symbols). The wavenumber of a-top CO corresponding to CO(1) downshifts by only 4 cm^{-1} in the interval of CO coverage from 1.0 to 0.31 and then drops down to attain $\nu_{CO_L} = 2036\ cm^{-1}$ at $X_{CO} = 0.11$. Meanwhile, the CO-(2) population demonstrates quite different coverage dependence. Indeed, its wavenumber downshifts by 24 cm^{-1} with the coverage decrease from 1.0 to 0.54, staying unchanged at 2013 $\pm$ 3 cm^{-1} upon further decrease of the coverage to ~0.11. This adds complementary spectroscopic evidence of different properties of the CO(1) and the CO(2) populations.

3.4. Discussion. *3.4.1. Intraparticle versus Interparticle Heterogeneity*. As shown in Section 3.3, both cyclic voltammetry as well as infrared spectroscopy suggest the existence of two different CO populations on Pt/Sibunit. CO(1) is oxidized at low overpotentials (LPP) and exhibits high vibrational frequencies, while CO(2) is oxidized at high overpotentials (HPP) and shows lower CO_L wavenumbers and different dependence on CO coverage. Let us analyze the experimental results and rationalize the effects of (i) intraparticle and (ii) interparticle heterogeneity on CVs and vibrational spectra of chemisorbed CO.

We start from the intraparticle heterogeneity concept. It is well established that CO binding energy is very sensitive to the type of the adsorption site on noble metal surfaces and increases with the decrease of metal coordination number. According to the density-functional calculations performed by Hammer et al.,[45] CO chemisorption energy increases from ~1.25 eV for a Pt(11 8 5) terrace site to 1.45 eV for a (111) terrace site, 1.55 eV for a (100) terrace site, 1.95 eV for a (11 8 5) step site, and 2.15 eV for a (11 8 5) kink site. Given different adsorption energy of CO on high and low coordination sites, Guerin et al.[12] attributed the low potential peak on E-TEK Pt/Vulcan catalyst to CO oxidation on terraces, while CO oxidized in the high potential peak to CO on the edges. This explanation is, however, not supported by the results of the present work.

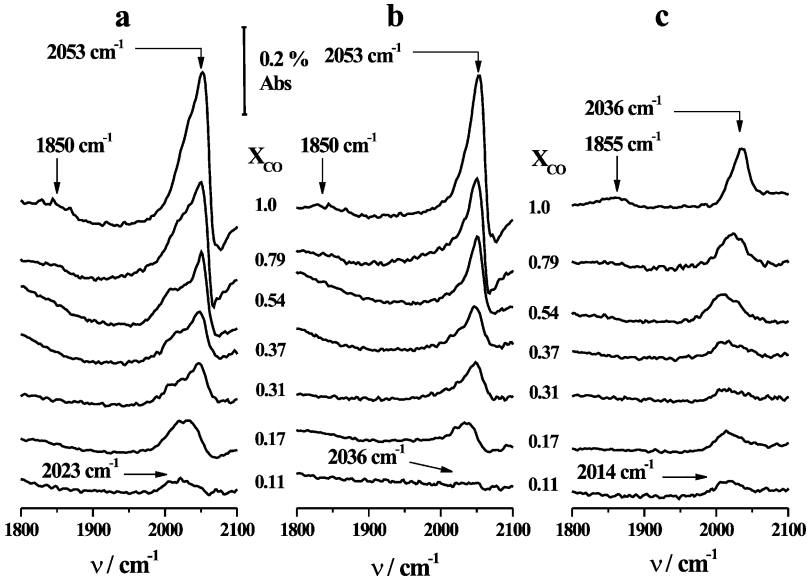

Figure 10. (a) FTIR spectra for different CO coverages (as indicated in the graph) established by CO dosing (see text for details). (b) and (c) show the IR spectra corresponding to CO(1) and CO(2) populations, respectively, and calculated using the procedure described in the text. All spectra were collected at 0.1 V vs RHE in 0.1 M $HClO_4$. The reference spectrum was collected at 0.1 V vs RHE after oxidizing CO at 1.2 V vs RHE for 60 s. CO adsorption potential 0.1 V vs RHE, T = 298 K.

As evidenced by Figure 5, LPP and HPP increase simultaneously. Meanwhile, if CO(2) corresponds to CO adsorbed on the edges, one would expect that because of the higher characteristic adsorption energy it is populated first. Indeed, on single crystal surfaces CO at low coverages adsorbs preferentially at low coordination sites, so that CO dosing results in sequential filling of first the step and only then the terrace sites, both at the solid/gas[14,15,46] as well as the solid/liquid interfaces.[17,20,47]

If we now try to rationalize CO stripping voltammograms obtained under stepwise oxidation conditions in the framework of intraparticle heterogeneity, we will have to assume that CO on particles' terraces can be fully oxidized, leaving CO on edges intact (see Figure 4). This could only be true if adsorbed CO were totally immobile, which is in contradiction with the previous knowledge. CO diffusion on single crystalline Pt is supposed to be fast. Koper et al.[48] have recently reported 10^{-11} cm^2 s^{-1} as a lower limit for the CO_{ads} diffusion coefficient at stepped Pt[n(111) $\times$ (111)] in contact with aqueous electrolytes. Our recent data on modeling CO oxidation kinetics on carbon-supported Pt nanoparticles[10] suggest that the CO diffusion coefficient is strongly particle size dependent, decreasing with the decrease in the particle size. For ~3 nm Pt particles, D_{CO} was estimated as $\geq 3 \times 10^{-13}$ cm^2 s^{-1}. An estimate of the average displacement of a CO molecule during the time of the potential step (300 s) gives $x \geq \sqrt{2D_{CO}t} \approx 1.3 \times 10^{-5}$ cm $= 130$ nm $\gg d_{Pt}$ which makes splitting the CO stripping peak into CO oxidation on terraces and on edges very unlikely.

In this context it is worth recalling that at saturation coverage CO oxidation on stepped Pt single crystals is observed as a single peak and does not split into separate peaks of CO on terraces and CO on steps. This is, apparently, a consequence of CO diffusion on the surface and exchange between terrace and step CO molecules. The position of the CO stripping peak shifts negative with the increase in the step density,[42] which is apparently caused by the fact that reactive OH_{ads} groups are preferentially generated at the low coordination sites. It has been suggested that CO oxidation occurs in a Langmuir−Hinshelwood reaction between oxygen species adsorbed at the step sites and CO molecules adsorbed on terraces both at the solid/gas[15] and solid/liquid electrified interfaces.[18] Petukhov et al.[49] and then Koper and co-workers[48,50] proposed mathematical models for CO oxidation on extended surfaces. The model described by Koper and co-workers[48,50] includes (i) preferential OH formation at the edge sites, (ii) fast CO diffusion on the terraces, (iii) exchange between terrace and edge CO, and (iv) CO oxidation upon a Langmuir−Hinshelwood reaction between edge OH and terrace CO and accounts well for the experimental data on CO stripping and chronoamperometry at stepped Pt surfaces.

Yates et al.[15] have provided strong evidence of CO displacement from the edge sites by adsorbed oxygen (for which the binding energy to Pt is higher than that for CO). From the CV in CO-free solution one may clearly see that 0.7 V is above the onset of oxygen adsorption (Figure 3). Thus, even if CO diffusion on Pt was very slow, one would expect that during the potential step to 0.7 V CO from the particle edges is displaced by the surface oxygen.

Another argument against the "terrace and edge" origin of the current peaks in the stripping CV is the following. Let us consider a 3.1 nm size Pt nanoparticle as an ideal cuboctahedron. Thus, it will comprise 162 atoms in (111) facets, 85 atoms in (100) facets, 127 edge atoms, and 11 corner atoms.[51,52] Now, assuming that the position of the oxidation peak on the potential scale is determined solely by the CO chemisorption energy (which as discussed above is greatly different for different terrace, step, and kink sites[45]) and there is no exchange between different adsorption sites (In this context it is worth mentioning that according to Koper et al.,[53] CO and OH chemisorption energies are closely related), we come to a conclusion that neglecting particle size distribution and the nonideal shape of Pt nanoparticles, one would expect at least four voltammetric peaks in the CV in accordance with the types of the adsorption sites on the surface.

We now move to the discussion of the IR spectra. The main contributions, which cause vibrational frequency shifts upon variation of CO coverage, are dipole−dipole coupling and chemical shifts. The latter arise from changes in the adsorbate bonding with the coverage and also include surface heterogeneity, that is, the presence of different adsorption sites. Hence, the singleton frequency of CO depends strongly on the coordination number n of the surface site to which it is adsorbed. For the Pt/gas interface the following relation has been established by Brand and co-workers[54,55] for linearly bonded CO singleton frequency: $\nu_S = 1997 + 10\ n$. However, observation of CO featuring singleton frequencies is only possible when the adsorbate vibrational coupling is minimized. Experimentally, singleton frequences are determined using isotope mixing (e.g., $^{12}CO/^{13}CO$) experiments by extrapolating ν_{CO} in dilute $^{12}CO/^{13}CO$ mixtures to zero ^{12}CO coverage (see, e.g., Chang and Weaver[19] and Kim et al.[20] and references therein). At high CO coverages, its vibrational spectra are dominated by dipole−dipole coupling of the adsorbate molecules. The dipole−dipole coupling between adsorbate molecules with similar frequencies leads to an increase in the observed absorbance compared to the sum of the individual absorbances, as well as an increase in the frequency of the synchronized vibrations. For adsorbate molecules with different frequencies, an additional effect is the intensity transfer from low to high wavenumbers. In the case of CO adsorption on stepped single crystals, dipole coupling between the terrace and step CO results in the intensity borrowing from the low frequency vibration of step CO to the high frequency vibration of terrace CO. This usually gives rise to a single narrow high frequency a-top CO band at high CO coverages. Lowering the coverage lifts vibrational coupling, and hence CO molecules adsorbed on different surface sites become discernible.

From the first glance, the evolution of the IR spectra with the decrease of CO fractional coverage under dosing conditions is similar to that observed for stepped single crystals and could be thus taken as an argument in favor of the intraparticle heterogeneity model. However, if one compares the spectra under stepwise oxidation and dosing conditions for Pt/Sibunit with those reported for Pt single crystals, one will notice major differences, which cannot be rationalized in the framework of intraparticle heterogeneity concept. Indeed, the results of this work show that for nanoparticles the red shift of the high frequency component upon coverage decrease under stepwise oxidation conditions is much higher compared to the one under dosing experiments (the high frequency band in the latter case stays nearly unchanged at 2051 ± 2 in the coverage interval from 1.0 to 0.31), while the band splitting is stronger in the latter case. This is in contrast to the data published for single crystal surfaces, which showed much larger red shifts under dosing conditions.[17,19,20,47] For single crystal electrodes, the differences in the extent of vibrational coupling for CO adlayers prepared by oxidative stripping and dosing have been reconciled

by invoking CO island formation. It has been suggested that the size of the islands depends on the prehistory of the adlayer. When CO fractional coverages are established by dosing, adsorption occurs at random and small CO islands are formed (this is particularly true for the adsorption in the H_{UPD} region due to the H coadsorption). Meanwhile, under the oxidative stripping conditions, CO oxidation is believed to occur at the rims of the CO islands, supposedly resulting in their larger size. Hence, if we neglect the particle size distribution and assume that the evolution of the IR spectra for Pt nanoparticles with the decrease of X_{CO} results solely from lifting vibrational coupling between CO molecules adsorbed on terrace and edge sites, we will come to a contradiction between the pronounced band splitting and the small red shift of ν_{CO_L} under dosing conditions (smaller than under stepwise oxidation). This contradiction cannot be reconciled in the framework of the intraparticle heterogeneity model.

We now come to the analysis of the results in terms of interparticle heterogeneity, thus assuming that the HPP and the low frequency vibrational band correspond to CO adsorbed on "small" particles, while the LPP and the high frequency vibrational band correspond to CO adsorbed on "large" particles. This attribution is supported by the bimodal size distribution of the catalyst under study (Figure 2), comprising "large" ($d \sim$ 3.6 nm) and "small" ($d \sim$ 1.7 nm) Pt particles, and by our previous findings on the influence of particle size on the overpotential of CO oxidation on Pt. Indeed, we have recently demonstrated[10] that CO_{ads} oxidation overvoltage increases when the particle size decreases below approximately 3 nm, while for larger particles the size dependence levels off, so that the CO stripping peak from nanoparticles above 3 nm in diameter is observed at the same potential as that from CO oxidation on bulk polycrystalline Pt.[10] This attribution is supported by comparing the CO stripping charge under the HPP, which constitutes ~15% of the overall CO stripping charge, and the contribution of the particles $\leq$2 nm diameter to the overall surface area of nanoparticles of 19%. The increase of the CO oxidation overpotential with the decrease of the particle size results in preferential oxidation of CO on "large" particles, when potential is stepped to 0.7 V, and explains the evolution of the CVs upon stepwise oxidation (Figure 4). According to TEM data, Pt particles are uniformly dispersed on the carbon surface (Figure 1), and there is no direct contact between them. This precludes "communication" between nanoparticles (unless CO spills over to the carbon support, which is rather unlikely in view of its weak interaction with the graphite surface). Ultimately, stepwise oxidation at 0.7 V leads to complete removal of CO from the surfaces of the "large" particles and leaves CO on "small" particles intact. The latter stays on the surface until the potential is increased above the onset of CO oxidation on "small" nanoparticles, which according to our data is above 0.9 V.

Dosing experiments can also be readily explained in the framework of the interparticle heterogeneity model. Since CO adsorption energy on Pt is high, upon dosing, CO will be adsorbed at random on the surface of either large or small particles, depending on which it hits first. In case of an absence of spillover of CO from Pt to the Sibunit surface (which is supported by the data of the present work), equilibration of the CO adlayers between different particles is possible only via CO desorption/adsorption. Meanwhile, CO desorption from Pt is negligible at room temperature both at the solid/liquid[56] and the solid/gas interface.[57] The issue of CO desorption has been extensively discussed recently.[58] Davies et al.[59] based on the $^{13}CO/^{12}CO$ exchange experiments the claim that the CO desorption rate on Pt may be substantial even at room temperature. We would like, however, to make a distinction between the desorption process (which results in a decrease of CO coverage and which is relevant to our discussion) and the exchange process, which is well known in surface science and catalysis (see, e.g. Cuo et al.[60] and references therein), occurs between the adsorbed and bulk molecules (in the gas or solution phase), and does not result in a decrease of the overall adsorbate coverage (and is thus not relevant to our discussion). Negligible CO desorption under the experimental conditions employed results in simultaneous, rather than sequential, filling of the surface of "small" and "large" particles with CO upon dosing and thus a simultaneous increase of the HPP and LPP in stripping voltammograms (Figure 5). A similar phenomenon observed at the interface between silica supported Pt catalysts and gaseous CO has been denoted as "nonequilibrated" adsorption.[57]

The vibrational frequencies of 2054 and 2036 cm^{-1} found in this work at saturation CO coverage for CO(1) and CO(2) populations are in good agreement with their attribution to CO adsorbed on ~3.6 and ~1.7 nm nanoparticles, respectively. Indeed, the wavenumber of a-top CO adsorbed on Pt nanoparticles has been found to strongly depend on the particle size, decreasing for nanoparticles below 4 nm in size.[23] Different explanations have been offered to account for this observation, including (i) increase of the contribution of low coordination sites with the decrease of the particle size,[22,23] (ii) metal−support interaction,[7,61] and (iii) decrease of the extent of the vibrational coupling due to the "roughness" of the surface of nanoparticles.[22] The full width at half-maximum (fwhm) for both "large" and "small" Pt particles at saturation coverage constitutes approximately 30 cm^{-1}, (which is somewhat smaller than the values reported for supported Pt catalysts in the literature[22,23]).

Since, upon dosing, the CO populations on "large" and "small" particles rise simultaneously, the intensities of the bands corresponding to these populations will increase in parallel. This, obviously, explains the band splitting in Figure 10a. It is apparent from Figures 9a and 10 that the change of CO coverage produces different effects on the vibrational frequencies of CO adsorbed on "large" and "small" particles. The latter results from dipole−dipole coupling of CO molecules and will be discussed in detail in the following section.

The differences between the IR spectra obtained upon dosing and stepwise oxidation arise from the fact that in the latter case the CO population on "large" particles gradually decreases, resulting in a red shift of the CO vibrational frequency, while the population, and thus the wavenumber of CO adsorbed on "small" particles, does not change. This leads to a gradual decrease of ν_{CO_L} in the spectra of Figure 6a.

Before we move on, we would like to stress that the influence of the interparticle heterogeneity is not a unique property of the catalyst studied in this work, but rather it is a common feature of all supported metal catalysts (commercial as well as model). Even when the particle size distribution is rather narrow, its influence cannot be neglected if the properties of the catalyst are strongly dependent on the particle size. Since the smaller the size of the metal crystallites the stronger the size effects are, the more the behavior of a catalyst may be influenced by the size distribution. On the other hand, the bimodal size distribution of the catalyst used in this work assisted in highlighting the influence of interparticle heterogeneity on the electrochemical behavior and vibrational spectra. This makes our work particularly important for the interpretation of FTIR spectra of CO adsorbed on nanometer-sized electrocatalysts and

stresses the need of considering interparticle heterogeneity to achieve a better understanding of the particle size effects in electrocatalysis.

3.4.2. Vibrational Coupling of CO Molecules Adsorbed on Pt Nanoparticles. This work for the first time provides evidence of the influence of the particle size on the adsorbate vibrational coupling. Let us refer back to the ν_{CO_L} versus X_{CO} plots for "large" and "small" particles under dosing conditions (Figure 9a, filled symbols). Similarly to what has previously been observed for extended surfaces, ν_{CO_L} increases for both "large" and "small" particles as CO coverage is increased. Low energy features at low CO coverages ($\sim$2036 cm^{-1} for "large" and $\sim$2013 cm^{-1} for "small" particles) obviously correspond to CO adsorbed on low coordination sites. Hence, this work provides evidence for the preferential adsorption of CO at low coordination sites of nanometer-sized Pt electrocatalyst at low CO coverages. For "large" particles, an abrupt increase of ν_{CO_L} occurs between $X_{CO} = 0.2$ and $X_{CO} = 0.3$, while for "small" particles ν_{CO_L} increases only above $X_{CO} = 0.54$. These differences can be rationalized in terms of the different proportion of edge and terrace sites on the surfaces of these particles. Indeed, the ratio of edge and corner atoms to the total amount of surface atoms equals approximately 0.25 for 3.4 nm and 0.5 for 1.7 nm cuboctahedral Pt particles.[51,52] The change in the ν_{CO_L} versus X_{CO} slope and its correlation with the proportion of the edge sites for "large" and "small" particles is remarkable. Apparently, at high CO coverages, CO molecules adsorbed at the facets and CO molecules adsorbed at the edge sites are vibrationally coupled and give rise to a single absorption band, which for 3.6 nm particles lies at 2053 cm^{-1}, while for 1.7 nm particles it occurs at 2036 cm^{-1}. In this context it should be stressed that to achieve submonolayer CO coverages in this work we varied the concentration of CO in the "dosing" solution, keeping the time of adsorption constant and equal to 1 h to let the adlayer equilibrate. This procedure is different from the one employed in previous publications[17,19] where the adsorption time was varied for attaining fractional CO coverages. The independence of ν_{CO_L} on the coverage for particles <2 nm in size in a large coverage interval from 0.54 to 0.11 is not fully understood yet. Does the band at 2013 $\pm$ 3 cm^{-1} correspond to the vibrations of individual CO molecules or to the vibrations of vibrationally coupled molecules adsorbed at the particle edges? The first hypothesis seems to be more likely in view of the weak dipole−dipole coupling of adsorbate molecules adsorbed along the step edges of high index single crystals.[62]

Vibrational coupling of the adsorbate molecules on nanometer-sized particles is a very important, albeit insufficiently explored, issue. Its detailed analysis requires isotope mixing experiments and will be provided in a forthcoming publication. Here, we give a qualitative consideration to this matter. Of interest is a very small (4 cm^{-1}) downshift of ν_{CO_L} for "large" particles in the interval of X_{CO} from 1.0 to 0.31 under dosing conditions. Note that Korzeniewski et al.[17]observed an approximately 15 cm^{-1} red shift of ν_{CO_L} for Pt(557) and Pt(335) upon an X_{CO} decrease from 1.0 to $\sim$0.5. It is thus likely that CO adsorbed on Pt nanoparticles is subject to stronger vibrational coupling than CO adsorbed at single crystal surfaces. This means that clustering of CO molecules into islands occurs on 3 nm particles at low adsorbate coverages at 0.1 V RHE under dosing conditions, contrary to what has been observed for extended surfaces.[19] Strong coupling of CO molecules adsorbed on the facets of small metal particles is in agreement with the observation (which has been made both in surface science[14] and electrochemistry[17]) that the narrower the terrace, the larger is the extent of the adsorbate vibrational coupling. A number of possible reasons has been invoked in order to account for this phenomenon (see, e.g., Xu and Yates[14]), in particular (i) scaling the adsorbate−adsorbate separation distance down with the step width, (ii) electrostatic field effects, (iii) diminishing the difference between the singleton frequencies of CO adsorbed on the edge and on the terrace sites with narrowing the terraces down, and (iv) increase in the absolute CO coverage with the increase in the step density. The latter is at least in part due to the ability of CO molecules to tilt along the step edges, thus minimizing repulsive forces between the adjacent adsorbates.[62] CO island formation on metal nanoparticles has been previously invoked in heterogeneous catalysis.[63]

Although formation of compressed CO islands on metal surfaces has been known for a long time, its driving force is not fully understood yet. A number of possible reasons have been proposed and will be briefly discussed here. It is well established that the heat of CO adsorption is coverage dependent and, for example, for the Pt(111) plane it decreases from approximately 140 kJ mol^{-1} at low CO coverage to approximately 40−80 kJ mol^{-1} at saturation coverage.[36] This is a result of repulsive lateral adsorbate−adsorbate interactions between CO molecules. The latter, however, will not favor formation of compressed CO islands with high local coverage. Kato et al.[64] have recently brought forward an idea of the existence of attractive lateral interaction between CO molecules, in addition to through-space and through-substrate repulsive interactions between them. A possible origin of the latter is proposed to be either van der Waals interactions or direct chemical interactions between CO molecules through the extended metal 2π orbital. Hence, attractive lateral interactions between CO molecules may justify the CO island formation. Another possible reason is surface reconstruction and its lifting upon CO adsorption observed at the metal/UHV interface. Indeed, from the three low index planes of Pt, only (111) is known to be stable in UHV, whereas the two more open (100) and (110) surfaces reconstruct into a quasi-hexagonal "hex" and (1×2) "missing row" geometry, respectively, because of the lower surface energy of the latter structures compared to the original (1×1).[36] The surface phase transition "hex" $\leftrightarrow$ (1×1) was proven to occur upon CO adsorption on Pt(100), the difference in the heat of CO adsorption between "hex" and (1×1) structure being proposed as the driving force.[65] Similar surface phase transitions from $(1 \times 2) \leftrightarrow (1 \times 1)$ or (2×1)−p1g1− were also observed upon CO adsorption on Pt(110).[66,67] Such reconstructions lead to more open surfaces and diminish repulsive lateral interactions between CO molecules, giving rise to CO island formation. Note, however, that for Pt single crystals surface phase transitions seem to be inherent to UHV. Hence, Marković and co-workers[68,69] found that Pt(111) (1×1), Pt(110) (1×2), and Pt(110) (1×1) are stable in the potential region between 0 and 1.0 V vs RHE and that CO adsorption does not induce the $(1 \times 2) \leftrightarrow (1 \times 1)$ surface reconstructions observed in UHV. The situation may, however, change for nanometer-sized supported metal nanoparticles, which experience significant strain due to intrinsic size effects and interaction with support.[2,3] Adsorption releases the strain and may thus affect the surface structure and the shape of metal crystallites. The latter has been confirmed both theoretically and experimentally.[2,3,70] Another possible explanation for the formation of close-packed CO islands could be attractive lateral interactions between solvent molecules and anions (hydrogen bonding), adsorbed at the interface, which expel CO molecules and force them to compress into islands. As stressed by Zhdanov et al.,[71] lateral interactions between adsorbates of the order of as little as $\sim$4 kJ mol^{-1} may be sufficient for the island formation. The

presence of solvent molecules is likely to exert a significant influence on the adsorbate−substrate and adsorbate−adsorbate interactions and is one of the main reasons for the differences observed between the adlayer structures in UHV and in the electrochemical environment.[72] Chang and Weaver[19] suggested that these are repulsive forces between CO and water molecules that stabilize CO islands on noble metal surfaces.

3.4.3. Influence of the Particle Size on CO Adsorption and Oxidation. The results of this work demonstrate considerable differences between "large" and "small" nanoparticles in terms of (i) CO oxidation overpotential, (ii) vibrational frequencies of adsorbed CO molecules, and (ii) their dipole−dipole coupling. The increase in CO oxidation overpotential has been discussed in our previous publication.[10] This is likely to originate from stronger bonding of CO to the surface, concomitant decrease of CO_{ads} diffusion coefficient, and slow kinetics of reactive OH groups generation. The red shift of the wavenumber of adsorbed CO with the decrease of particle size has been discussed in previous publications,[22,23,61] but its reasons are not completely clear yet. It is remarkable that the difference in the particle size of ~2 nm results in a drastic change of both CO oxidation overpotential and CO vibrational frequency. The latter may be related to differences in the crystalline structure between "large" and "small" particles (cf. Section 3.1) and requires further investigation. As discussed above, the extent of the adsorbate vibrational coupling depends on the particle size and the ratio of adsorption sites of different coordination.

Some important conclusions concerning the mechanism of CO oxidation on "large" and small" particles emerge from the difference spectra represented in Figure 8. As evidenced by the figure, CO oxidized in the first potential step (20 s at 0.7 V) features a narrow IR band with high wavenumber (2057 cm^{-1}). As the oxidation proceeds, ν_{CO_L} gradually decreases (Figure 9a, open symbols) while the bandwidth increases (Figure 9b). The upper branch of the ν_{CO_L} versus X_{CO} plot for the difference spectra is strikingly similar to the ν_{CO_L} versus X_{CO} plot for "large" particles under dosing conditions (cf. open and filled symbols in Figure 9a). This proves that in the course of oxidation CO molecules are first removed from the facets of large particles (strongly coupled CO molecules with high ν_{CO_L}). A decrease in the amount of CO molecules on the particle facets leads to a gradually lifting dipole−dipole coupling and hence results in a decrease of ν_{CO_L} and an increase of fwhm. The difference spectra corresponding to the further oxidation steps (Figure 8, X_{CO}: 0.23 → 0.17 and X_{CO}: 0.17 → 0.16) apparently involve an increasing contribution from CO molecules adsorbed at particle edges. After the CO on "large" particles is oxidized, the step potential is increased and the oxidation of CO on "small" particles sets in. This is reflected in a sudden drop of the fwhm (Figure 9b). It is remarkable that CO oxidation on 1.7 nm nanoparticles also starts with a narrow peak, which then broadens. Obviously, CO oxidation on small particles also starts from the facets and then propagates to the edges. It should be stressed, however, that since spectra were acquired after stepping to 0.1 V, some rearrangements in the adsorbate layer during the spectra acquisition cannot be ruled out.

3.4.4. Nanoparticles versus Extended Surfaces. Probing CO adsorption and oxidation on carbon-supported Pt nanoparticles using FTIR and stripping voltammetry points to a number of similarities as well as disparities between nanoparticles and extended surfaces. Similar to extended single crystalline Pt surfaces, nanoparticles adsorb (bi)sulfate anions, which increase the overpotential for CO monolayer oxidation. Previous publications demonstrated unambiguously that CO on nanoparticle surfaces is oxidized via the Langmuir−Hinshelwood mechanism,[9,10] but the reaction kinetics is particle size dependent and slows down when the particle size decreases below approximately 3 nm.[10] According to FTIR data, CO adsorbs on nanoparticles in a-top and bridge-bonded configurations; their characteristic frequencies, however, are red shifted versus corresponding values for single crystals. Similar to those for extended surfaces, infrared spectra of CO adsorbed on nanoparticles show marked CO coverage dependence, but its origin is not exactly the same and also includes the influence of inter- and intraparticle heterogeneity. This work shows that, similar to single crystal surfaces, the CO oxidation starts from terraces and then propagates to the edges. However, it is impossible to obtain separate current peaks in a cyclic voltammogram for the CO oxidation from terrace and edge atoms (it is also not possible to separately oxidize terrace and step CO molecules on single crystal surfaces), supposedly due to the adsorbate exchange between different surface sites. At variance with the single crystal surfaces, the CO adlayer on a nanoparticulate electrode is not equilibrated at room temperature, presumably because of the absence of CO diffusion between the particles via the carbon support. On the other hand, within a single particle the adlayer is likely to be equilibrated, since the FTIR spectra at low adsorbate coverages show CO molecules adsorbed first on the edges and only then on the facets. CO adsorbed on nanoparticles seems to experience much stronger vibrational coupling compared to CO on single crystal surfaces, which is likely to originate from the small dimensions of the facets on nanoparticle surfaces.

4. Conclusions

This paper provides evidence for an influence of intra- and interparticle heterogeneity on the vibrational spectra and cyclic voltammetry of CO adsorbed on nanometer-sized carbon-supported Pt particles. The latter is highlighted by the bimodal size distribution of Pt nanoparticles on Sibunit. We demonstrate that underestimation of the interparticle heterogeneity may result in misinterpretation of the experimental data. The peak splitting observed in CO stripping voltammetry for carbon-supported Pt nanoparticles is attributed to CO oxidation on nanoparticles of different sizes and not on their terraces and edges. This assignment is supported by concerted agreement of the results of FTIR and stripping voltammetry at submonolayer CO coverages obtained by CO dosing from diluted solutions and stepwise oxidation of saturated CO adlayers. The values of both the oxidation peak and the oxidation onset potential are particle size dependent and shift positively with the decrease in particle size. In this paper, we show for the first time the evidence for (bi)sulfate adsorption on Pt nanoparticles. The latter results in an increase of the CO oxidation potential apparently due to blocking the surface for oxygen adsorption. It is remarkable that (bi)sulfate adsorption exerts different influence on CO oxidation on large (3.6 nm) and small (1.7 nm) particles, the latter experiencing a much larger shift of the oxidation potential than the former. We demonstrate that CO can be fully removed from large (3.6 nm) particles after stepping at 0.7 V for 300 s, while CO on small particles is retained. This allows the separation of the contributions of large and small particles in the vibrational spectra.

CO is adsorbed on 3.6 and 1.7 nm nanoparticles in a-top and bridge-bonded configurations. At 0.1 V and saturation coverage, the ν_{CO_L} equals 2054 and 2036 cm^{-1} for 3.6 and 1.7 nm particles, respectively. We report here that both a-top and bridge-bonded CO are simultaneously removed from nanoparticle surfaces upon oxidation. Oxidation of CO on nanometer-sized particles starts at terraces of large particles, propagating to their edges and ultimately to the terraces and edges of small particles.

We show that CO dosing from dilute solutions results in a random adsorption on the surfaces of large and small particles, and there is no exchange and equilibration of the adlayers on different nanoparticles through the carbon support. This paper provides evidence concerning strong intermolecular vibrational coupling of CO adsorbed on the low and high coordinated sites of Pt nanoparticles. Adsorption of CO at low coverages occurs first on low coordinated surface sites and is characterized by low vibrational frequencies. Further adsorption leads to filling the adsorption sites on particle facets, which couple with the CO molecules on the edge sites, resulting in a single blue-shifted IR absorption band. An absence of clear IR band splitting into terrace and edge CO molecules likely originates from their strong vibrational coupling.

Acknowledgment. Financial support by the Deutsche Forschung Gemeinschaft (DFG) under contracts Sti74/8-4 and 436RUS113-718-1-1 and by HGF/BMBF/NRC (Contract No. 01SF 0201) is gratefully acknowledged. We thank K.A. Friedrich for his helpful cooperation and for letting us use his IR cell at the beginning of this work.

References and Notes

(1) *Catalysis & Electrocatalysis at Nanoparticle Surfaces*; Wieckowski, A., Savinova, E. R., Vayenas, C. G., Eds.; Marcel Dekker: New York, 2003.

(2) Henry, C. R. *Surf. Sci. Rep*. **1998**, *31*, 235.

(3) Henry, C. R. In *Catalysis & Electrocatalysis at Nanoparticle Surfaces*; Wieckowski, A., Savinova, E. R., Vayenas C. G., Eds.; Marcel Dekker: New York, 2003; p 239.

(4) Yudanov, I. V.; Sahnoun, R.; Neyman, K. M.; Roesch, N.; Hoffmann, J.; Schauermann, S.; Johanek, V.; Unterhalt, H.; Rupprechter, G.; Libuda, J.; Freund, H.-J. *J. Phys. Chem. B* **2003**, *107*, 255.

(5) Libuda J.; Meusel I.; Hoffmann J.; Hartmann J.; Piccolo L.; Henry C. R.; Freund H. J. *J. Chem. Phys.* **2001**, *114*, 4669.

(6) Santra, A. K.; Goodman, D. W. *Electrochim. Acta*. **2002**, *47*, 3595.

(7) Friedrich, K. A.; Henglein, F.; Stimming, U.; Unkauf, W. *Colloids Surf., A* **1998**, *134*, 193.

(8) Takasu, Y.; Zhang, X.-G.; Minoura, S.; Murakami, Y. *Appl. Surf. Sci*. **1997**, *121/122*, 596.

(9) Cherstiouk, O. V.; Simonov, P. A.; Zaikovskii, V. I.; Savinova, E. R. *J. Electroanal. Chem.* **2003**, *554*−*555C*, 241.

(10) Maillard, F.; Eikerling, M.; Cherstiouk, O. V.; Schreier, S.; Savinova, E.; Stimming, U. *Faraday Discuss.* **2004**, *125*, 357.

(11) Park, S.; Xie, Y.; Weaver, M. J. *Langmuir* **2002**, *18*, 5792.

(12) Guerin, S.; Hayden, B. E.; Lee, C. E.; Mormiche, C.; Owen, J. R.; Russell, A.; Theobald, B.; Thompsett, D. *J. Comb. Chem*. **2004**, *6*, 149.

(13) Zdhanov, V.; Kasemo, B. *Chem. Phys. Lett*. **2003**, *376*, 220.

(14) Xu, J.; Yates, J. T., Jr. *Surf. Sci.* **1995**, 327, 193.

(15) Yates, J. T., Jr. *J. Vac. Sci. Technol., A* **1995**, *13*, 1359.

(16) Chang, S.-C.; Weaver, M. J. *Surf. Sci.* **1990**, *230*, 222.

(17) Kim, C. S.; Korzeniewski, C. *Anal. Chem*. **1997**, *69*, 2349.

(18) Lebedeva, N. P.; Rodes, A.; Feliu, J. M.; Koper, M. T. M.; van Santen, R. A. *J. Phys. Chem. B* **2002**, *106*, 9863.

(19) Chang, S.; Weaver, M. J. *J. Chem. Phys*. **1990**, *92*, 4582.

(20) Kim, C. S.; Tornquist, W. J.; Korzeniewski, C. *J. Chem. Phys*. **1994**, *101*, 9113.

(21) Chang, S. C.; Weaver, M. J. *J. Phys. Chem*. **1991**, *95*, 5391.

(22) Friedrich, K. A.; Henglein, F.; Stimming, U.; Unkauf, W. *Electrochim. Acta* **2001**, *47*, 689.

(23) Park, S.; Wasileski, S. A.; Weaver, M. J. *J. Phys. Chem. B* **2001**, *105*, 9719.

(24) Park, S.; Tong, Y.-Y.; Wieckowski, A.; Weaver, M. J. *Electrochem. Commun.* **2001**, *3*, 509.

(25) Park, S.; Tong, Y. Y.; Wieckowski, A.; Weaver, M. J. *Langmuir* **2002**, *18*, 3233.

(26) Wasileski, S. A.; Koper, M. T. M.; Weaver, M. J. *J. Phys. Chem. B* **2001**, *105*, 3518.

(27) Pecharromán, C.; Cuesta, A.; Gutierrez, C. *J. Electroanal. Chem*. **2002**, *529*, 145.

(28) Pecharromán, C.; Cuesta, A.; Gutierrez, C. *J. Electroanal. Chem*. **2004**, *563*, 91.

(29) Yermakov, Yu. I.; Surovikin, V. F.; Plaksin, G. V.; Semikolenov, V. A.; Likholobov, V. A.; Chuvilin, A. L.; Bogdanov, S. V. *React. Kinet. Catal. Lett*. **1987**, *33*, 435.

(30) *Carbon Blacks*, 2nd ed.; Donnet, J. B., Bansal, R. Ch., Wang, M.-J. Eds.; Marcel Dekker: New York, 1993.

(31) Simonov, P. A.; Likholobov, V. A. In *Catalysis & Electrocatalysis at Nanoparticle Surfaces*; Wieckowski, A., Savinova, E. R., Vayenas, C. G., Eds.; Marcel Dekker: New York, 2003; p 409.

(32) Sun, S.-G.; Cai, W.-B.; Wan, L.-J.; Osawa, M. *J. Phys. Chem. B* **1999**, *103*, 2460.

(33) Maillard, F.; Martin, M.; Gloaguen, F.; Léger J.-M. *Electrochim. Acta* **2002**, *47*, 3431.

(34) Marković, N. M.; Ross, P. N. *Electrochim. Acta* **2000**, *45*, 4101.

(35) Cherstiouk, O. V.; Simonov, P. A.; Savinova, E. R. *Electrochim. Acta* **2003**, *48*, 3851.

(36) Marković, N. M.; Ross, P. N., Jr. *Surf. Sci. Rep.* **2002**, *45*, 117 and references therein.

(37) Magnussen, O. M. *Chem. Rev.* **2002**, *102*, 679.

(38) Funtikov, A. M.; Stimming, U.; Vogel, R. *J. Electroanal. Chem*. **1997**, *428*, 147.

(39) Clavilier, J.; El Achi, K.; Rodes, A. *J. Electroanal. Chem*. **1989**, *272*, 253.

(40) Clavilier, J.; Rodes, A. *J. Electroanal. Chem*. **1993**, *348*, 247.

(41) Palaikis, L.; Zurawski, D.; Hourani, M.; Wieckowski, A. *Surf. Sci*. **1988**, *199*, 183.

(42) Lebedeva, N. P.; Koper, M. T. M.; Herrero, E.; Feliu, J. M.; van Santen, R. A. *J. Electroanal. Chem.* **2000**, *487*, 37.

(43) Villegas, I.; Weaver, M. J. *J. Chem. Phys.* **1994**, *101*, 1648.

(44) Rush, B. M.; Reimer, J. A.; Cairns, E. J. *J. Electrochem. Soc*. **2001**, *148*, A137.

(45) Hammer, B.; Nielsen, O. H.; Nørskov, J. K. *Catal. Lett*. **1997**, *46*, 31.

(46) Xu, J.; Yates, J., Jr. *J. Chem. Phys*. **1993**, *99*, 725 and references therein.

(47) Kim, C. S.; Tornquist, W. J.; Korzeniewski, C. *J. Phys. Chem.* **1993**, *97*, 6484.

(48) Koper, M. T. M.; Lebedeva, N. P.; Hermse, C. G. M. *Faraday Discuss.* **2002**, *121*, 301.

(49) Petukhov, A. V.; Akemann, W.; Friedrich, K. A.; Stimming, U. *Surf. Sci*. **1998**, *402*−*404*, 182.

(50) Lebedeva, N. P.; Koper, M. T. M.; Feliu, J. M.; van Santen, R. A. *J. Phys. Chem. B* **2002**, *106*, 12938.

(51) van Hardeveld, R.; Hartog, F. *Surf. Sci*. **1969**, *15*, 189.

(52) McBreen, J.; Mukerjee, S. In *Interfacial Electrochemistry*; Wieckowski, A., Ed.; Marcel Dekker: New York, 1999; p 49.

(53) Koper, M. T. M.; Shubina; T. E.; van Santen, R. A. *J. Phys. Chem. B* **2002**, *106*, 686.

(54) Brandt, R. K.; Sorbeilo, R. S.; Greenler, R. G. *Surf. Sci*. **1992**, *271*, 605.

(55) Brandt, R. K.; Hughes, M. R.; Bourget, L. P.; Truszkowska, K.; Greenler, R. G. *Surf. Sci.* **1993**, *286*, 15.

(56) It is common knowledge in electrochemistry that CO adlayers on Pt electrodes are extremely stable in the potential region below the oxidation onset unless traces of oxygen penetrate into the electrochemical cell.

(57) Podkolzin, S. G.; Shen, J.; de Pablo, J. J.; Dumesic, J. A. *J. Phys. Chem.* **2000**, *104*, 4169.

(58) *Workshop on Theory and Surface Measurements in Fuel Cell Catalysis*, Denmark, June 16−18, 2003, http://www.scs.uiuc.edu/wieckowski/Lyngby/Lyngby.html.

(59) (a) Davies, J. C.; Nielsen, R. M.; Thomsen, L. B.; Chorkendorff, I.; Logadóttir, Á.; Łodziana, Z.; Nørskov, J. K.; Li, W. X.; Hammer, B. accepted to *Fuel Cells: From Fundamentals to Systems*, (b) Wieckowski, A. et al. using radiolabeling method observed fast decrease in the ^{14}CO coverage upon introducing ^{12}CO to the solution.

(60) Cuo, X.; Xin, M.; Zhai, R. *J. Phys. Chem*. **1994**, *98*, 7175.

(61) Rice, C.; Tong, Y. Y.; Oldfield, E.; Wieckowski, A.; Hahn, F.; Gloaguen, F.; Léger, J.-M.; Lamy, C. *J. Phys. Chem. B* **2000**, *104*, 5803.

(62) Henderson, M. A.; Szabo, A.; Yates, J. T. *J. Chem. Phys.* **1989**, *91*, 7245.

(63) Fanson, P. T.; Delagss, N. W.; Lauterbach, J. *J. Catal*. **2001**, *204*, 35.

(64) Kato, H. S.; Okuyma, H.; Yoshinobu, J.; Kawai, M. *Surf. Sci*. **2002**, *513*, 239.

(65) (a) Behm, R. J.; Thiel, P. A.; Norton, P. R.; Ertl, G. *J. Chem. Phys*. **1983**, *78*, 7437. (b) Thiel, P. A.; Behm, R. J.; Norton, P. R.; Ertl, G. *J. Chem. Phys*. **1983**, *78*, 7448.

(66) Hoffmann, P.; Bare, S. R.; King, D. A. *Surf. Sci.* **1982**, *117*, 245.

(67) Jackman, T. E.; Davies, J. A.; Jackson, O. P.; Unertl, W. N.; Norton, P. R. *Surf. Sci*. **1982**, *120*, 389.

(68) Marković, N. M.; Grgur, B. N.; Lucas, C. A.; Ross, P. N. *Surf. Sci.* **1997**, *384*, L805.

(69) Lucas, C. A.; Marković, N. M.; Ross, P. N. *Surf. Sci*. **1999**, *425*, L381.

(70) Zhdanov, V. P.; Kasemo, B. *Phys. Rev. Lett*. **1998**, *81*, 2482.

(71) Zdhanov, V.; Kasemo, B. *Surf. Sci*. **2003**, *545*, 109.

(72) Weaver, M. J. *Surf. Sci*. **1999**, *437*, 215.